Optimal Updating of INS Using Sighting Devices

Itzhack Y. Bar-Itzhack*
Technion – Israel Institute of Technology, Haifa, Israel

A low-accuracy inexpensive Intertial Navigation System (INS), which is mounted on board a moving vehicle, is updated using information from an onboard sighting device (SD). Two updating modes are considered. The first mode utilizes the deviation of landmarks from their INS-computed location in the field of view of the SD. The second mode utilizes the deviation of the angular rate of the SD, when locked on landmarks, from its INS-computed value. A suboptimal extended Kalman filter is designed for this system. The observation equations are developed and linearized for both updating modes. A covariance analysis is performed and results of computer runs are displayed and analyzed.

I. Introduction

IN the absence of other suitable navigational aids, an intertial navigation system (INS) of some kind has to be used on board flight vehicles whose accuracy is an important factor. An unfortunate feature of an INS is its error divergence with time. This disadvantage may be overcome by either using a highly accurate INS or by periodically updating an inaccurate INS if updating is a viable option. The latter is certainly a more desirable choice, since an accurate INS is a costly system. This consideration is particularly important in relatively inexpensive vehicles.

A well-known approach is to fly over an identifiable object and update the INS when passing directly overhead. The updating method analyzed in this work allows the vehicle to keep its course. Therefore, the measured quantities used for updating are angular quantities. A convenient updating mode can be used in vehicles which carry a sighting device (SD) like radar or optical devices. There is a relationship between the position of a landmark in the field of view relative to the line of sight (LOS) of the SD, after the latter is aimed at the assumed position of the landmark, and the INS error. This relationship can be used for an optimal estimation of the INS errors and of the values of its error sources.

Another updating mode is to lock the LOS on a landmark whose location is either known or estimated, measure yaw and pitch rates of the SD, and then compare them to the corresponding INS-computed rates. The difference between the corresponding angular rates is related to the INS error. This relationship can be used, too, to estimate the INS errors and the values of its error sources.

INS updating using LOS and either star or landmark sighting information in some fashion has been investigated, to a certain extent, in the literature in the past.[1-4] The present study presents a detailed covariance analysis where the estimated INS errors and error sources are propagated and updated using the extended Kalman filter.

II. Linearized Observation Equations

Mode I: Errors in the Field of View

Consider Fig. 1 where the l system denotes the local-level local-north coordinate system, not shown in Fig. 1, whose x axis coincides with the LOS in the SD. When the vehicle cruises between landmarks the s coordinate system coincides with the l system and when the vehicle reaches the vicinity of a landmark the computer computes two Euler angles which are the azimuth and the depression angles at which the s system has to be rotated away from the $\bar{\omega}$ system such that the x axis of the s system (the LOS) will point at the landmark. When the INS is error-free these angles are correctly computed as β_0 and α_0 and the s coordinate system of the SD is rotated correctly into the s_0 coordinate system whose x axis does indeed point at the landmark. Then

$$r^l_{s0} = [\,|\bar{r}|, \quad 0, \quad 0] \tag{1}$$

where r_{s0} is a column vector whose elements are, respectively, the x, y, and z components of $\bar{r}$ when resolved in the s_0 coordinate system.

In reality the INS computes an erroneous position P_c and hence the computed Euler angles are β_c and α_c, respectively. Moreover, the platform coordinate system p does not coincide with the l system, and since the p system is mistaken by the hardware for the l system, it turns the SD away from the p rather than from the l system. In conclusion, the SD is turned away erroneously from the p system by the two erroneous Euler angles β_c and α_c. This brings the coordinate system of the SD into coincidence with the Cartesian coordinate system s_c. The transformation matrix from the l to the s_c system D^l_{sc} can be computed as follows:

$$D^l_{sc} = D^p_{sc} D^l_p \tag{2}$$

where D^l_p is the transformation matrix from the l to the p system and is expressed in terms of the platform misalignment angles as follows

$$D^l_p = \begin{bmatrix} 1 & \phi_z & -\phi_y \\ -\phi_z & 1 & \phi_x \\ \phi_y & -\phi_x & 1 \end{bmatrix} \tag{3}$$

where

$$\phi_x = \psi_x - \Delta y/(R_E + H) \tag{4a}$$

$$\phi_y = \psi_y + \Delta x/(R_N + H) \tag{4b}$$

and

$$\phi_z = \psi_z - [\Delta y/(R_E + H)]\tan\lambda \tag{4c}$$

Presented as Paper 77-1107 at the AIAA 1977 Guidance and Control Conference, Hollywood, Fla., Aug. 8-10, 1977; submitted Aug. 12, 1977; revision received Jan. 23, 1978.

Index categories: LV/M Guidance; Sensor Systems; Guidance and Control.

*Senior Lecturer, Department of Aeronautical Engineering; presently on sabbatical leave with The Analytic Sciences Corporation (TASC) Reading, Mass. Member AIAA.

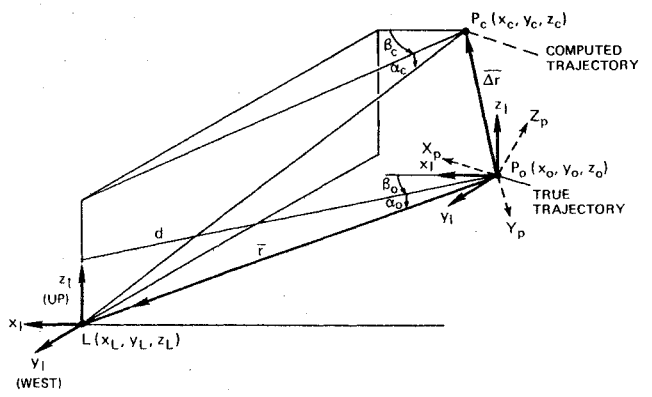

Fig. 1 The relative position P of the vehicle with respect to its computed position P_c and to the landmark L.

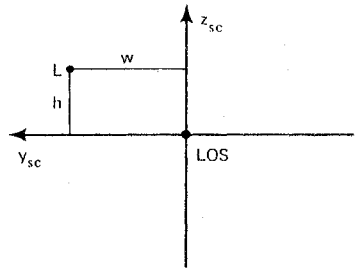

Fig. 2 The relative position of the landmark L with respect to the LOS in the "image plane."

where λ is the latitude angle, R_E is the eastbound radius of curvature of the Earth, R_N is the northbound radius of curvature of the Earth, and H is the altitude of the vehicle. The matrix D^p_{sc} is a function of β_c and α_c, and from Fig. 1 and from the definition of D^p_{sc} it is obvious that

$$D^p_{sc} = D(\beta_c, \alpha_c) = \begin{bmatrix} C\beta_c \cdot C\alpha_c & S\beta_c \cdot C\alpha_c & -S\alpha_c \\ -S\beta_c & C\beta_c & 0 \\ C\beta_c \cdot S\alpha_c & S\beta_c \cdot S\alpha_c & C\alpha_c \end{bmatrix} \tag{5}$$

where S denotes the sine function and C the consine function. When $\bar{r}$ is now resolved in the s coordinate system and arranged in a column vector the following expression is obtained

$$r^t_{sc} = [r_{xsc}, w, h] \tag{6}$$

As illustrated in Fig. 2, w and h are the coordinates of the landmark in the "image plane." They constitute the observation vector which reflects on the INS error and on the pointing error which stems from the inaccuracy of the pointing system of the SD. It should be noted that when all of the errors vanish, both w and h are zero as indicated in Eq. (1). This does not include the SD errors which are of stochastic nature and will be added later as observation noise.

Next, the measurement matrix H, which relates w and h with the INS errors, is developed. As seen in Eq. (6), the quantities w and h are embedded in r_{sc} which is related to r_l through

$$r_{sc} = D^p_{sc} D^l_p r_l \tag{7}$$

where from Fig. 1

$$r_l = \begin{bmatrix} x_L - x_0 \\ y_L - y_0 \\ z_L - z_0 \end{bmatrix} \tag{8}$$

From Eq. (3)

$$D^l_p = I - [\phi] \tag{9}$$

where I is the identity matrix and

$$[\phi] = \begin{bmatrix} 0 & -\phi_z & \phi_y \\ \phi_z & 0 & -\phi_x \\ -\phi_y & \phi_x & 0 \end{bmatrix} \tag{10}$$

As indicated by Eq. (5), D^p_{sc} is a function of β_c and α_c only; it can be expanded into a Taylor series about β_0 and α_0. Truncation of this series to exclude second- and higher-order terms yields

$$\begin{aligned} D^p_{sc} &= D(\beta_c, \alpha_c) = D(\beta_0 + \Delta\beta, \alpha_0 + \Delta\alpha) \\ &\approx D(\beta_0, \alpha_0) + \frac{\partial D}{\partial \beta}\Big|_{\beta_0,\alpha_0} \Delta\beta + \frac{\partial D}{\partial \alpha}\Big|_{\beta_0,\alpha_0} \Delta\alpha \end{aligned} \tag{11}$$

Denote

$$D_\beta = \frac{\partial D}{\partial \beta}\Big|_{\beta_0,\alpha_0} \tag{12a}$$

and

$$D_\alpha = \frac{\partial D}{\partial \alpha}\Big|_{\beta_0,\alpha_0} \tag{12b}$$

then Eq. (11) can be written as

$$D^p_{sc} = D(\beta_c, \alpha_c) = D(\beta_0, \alpha_0) + D_\beta \Delta\alpha + D_\alpha \Delta\alpha \tag{13}$$

Substitution of Eqs. (9) and (13) into Eq. (7) yields

$$r_{sc} = [D(\beta_0, \alpha_0) + D_\beta \Delta\beta + D_\alpha \Delta\alpha]\,(I - [\phi])\, r_l \tag{14}$$

which, after expansion and omission of second-order terms, becomes

$$r_{sc} = D(\beta_0, \alpha_0) r_l + D_\beta r_l \Delta\beta + D_\alpha r_l \Delta\alpha - D(\beta_0, \alpha_0)\,[\phi]\, r_l \tag{15}$$

The first term on the right-hand side of Eq. (15) is the error-free term, that is

$$D(\beta_0, \alpha_0) r_l = r_{s0} \tag{16}$$

and from Eq. (1), the second and third components of r_{s0} are zero, as expected. Therefore the second and third terms in the column vector δr defined by

$$\delta r = r_{sc} - D(\beta_0, \alpha_0) r_l \tag{17}$$

are w and h, respectively. This can be verified by inspection of Eq. (6). Combining Eqs. (15) and (17) yields

$$\delta r = D_\beta r_l \Delta\beta + D_\alpha r_l \Delta\alpha - D(\beta_0, \alpha_0)\,[\phi]\, r_l \tag{18}$$

In order to obtain the expression for w and h as a function of the INS errors, the right-hand side of Eq. (18) is now developed. From Fig. 1 it is realized that

$$\beta_0 = \tan^{-1}(y_L - y_0)/(x_L - x_0) \tag{19}$$

and that

$$\alpha_0 = \tan^{-1}(z_L - z_0)/d_0 \tag{20}$$

where

$$d_0 = [(x_L - x_0)^2 + (y_L - y_0)^2]^{1/2} \tag{21}$$

Differentiation of β_0 and α_0 yields

$$\Delta\beta = \beta_x \Delta x + \beta_y \Delta y \tag{22}$$

where

$$\beta_x = S(2\beta_0)/2(x_L - x_0) \tag{23a}$$

$$\beta_y = -C^2\beta_0/(x_L - x_0) \tag{23b}$$

$$\Delta\alpha = \alpha_x \Delta x + \alpha_y \Delta y + \alpha_z \Delta z \tag{24}$$

in which

$$\alpha_x = (z_0 - z_L)(x_L - x_0) C^2\alpha_0/d_0^3 \tag{25a}$$

$$\alpha_y = (z_0 - z_L)(y_L - y_0) C^2\alpha_0/d_0^3 \tag{25b}$$

$$\alpha_z = C^2\alpha_0/d_0 \tag{25c}$$

Denote the column vector which contains the bottom two elements of the column vector $[\cdot]$ by $[\cdot]_2$; then from the form of Eq. (5) and using Eqs. (8, 19 and 20) it can be shown that

$$[D_\beta r_l]_2 = \begin{bmatrix} d_{\beta_l} \\ 0 \end{bmatrix} \tag{26}$$

where

$$d_{\beta_l} = -C\beta_0 \cdot (x_L - x_0) - S\beta_0 \cdot (y_L - y_0) \tag{27}$$

It can be also shown that

$$[D_\alpha r_l]_2 = \begin{bmatrix} 0 \\ d_{\alpha_2} \end{bmatrix} \tag{28}$$

where

$$d_{\alpha_2} = C\beta_0 \cdot C\alpha_0 \cdot (x_L - x_0) + S\beta_0 \cdot C\alpha_0 \cdot (y_L - y_0) - S\alpha_0 \cdot (z_L - z_0) \tag{29}$$

Equations (5) and (10) yield

$$-[D(\alpha_0,\beta_0)[\phi] r_l]_2 = \begin{bmatrix} d_{11} & d_{12} & d_{13} \\ d_{21} & d_{22} & d_{23} \end{bmatrix} \phi \tag{30}$$

where, using Eqs. (8, 19 and 20) it is found that

$$d_{11} = C\beta_0 \cdot (z_L - z_0) \tag{31a}$$

$$d_{12} = S\beta_0 \cdot (z_L - z_0) \tag{31b}$$

$$d_{13} = -[C\beta_0 \cdot (x_L - x_0) + S\beta_0 \cdot (y_L - y_0)] = d\beta_l \tag{31c}$$

$$d_{21} = S\beta_0 \cdot S\alpha_0 \cdot (z_L - z_0) - C\alpha_0 \cdot (y_L - y_0) \tag{31d}$$

$$d_{22} = C\alpha_0 \cdot (x_L - x_0) - C\beta_0 \cdot S\alpha_0 \cdot (z_L - z_0) \tag{31e}$$

$$d_{23} = 0 \tag{31f}$$

and ϕ is a column vector whose elements are given by Eq. (4). Now, after substituting Eq. (4) into Eq. (30), the following is obtained:

$$-[D(\alpha_0,\beta_0)[\phi] r_l]_2 = \begin{bmatrix} \dfrac{d_{12}}{R_N+H} - \dfrac{1}{R_E+H}(d_{11} + d_{13}\cdot\tan\lambda) & 0 & d_{11} & d_{12} & d_{13} \\ \dfrac{d_{22}}{R_N+H} - \dfrac{1}{R_E+H} d_{21} & 0 & d_{21} & d_{22} & 0 \end{bmatrix} \begin{bmatrix} \Delta r \\ \psi \end{bmatrix} \tag{32}$$

The combination of Eqs. (22) and (26) yields

$$[D_\beta r_l]_2 \Delta\beta = \begin{bmatrix} d_{\beta_l}\beta_x & d_{\beta_l}\beta_y & 0 \\ 0 & 0 & 0 \end{bmatrix} \Delta r \tag{33}$$

and that of Eqs. (24) and (28) yields

$$[D_\alpha r_l]_2 \Delta\alpha = \begin{bmatrix} 0 & 0 & 0 \\ d_{\alpha_2}\alpha_x & d_{\alpha_2}\alpha_y & d_{\alpha_2}\alpha_z \end{bmatrix} \Delta r \tag{34}$$

where $\Delta r' = [\Delta x, \Delta y, \Delta z]$. Finally, the substitution of Eqs. (32-35) into Eq. (18) and the addition of the observation noise vector v_l, which contains the SD error, yields

$$\begin{bmatrix} w \\ h \end{bmatrix} = \left[\begin{array}{c|c} H_1 & H_4 \end{array}\right] \begin{bmatrix} \Delta r \\ \psi \end{bmatrix} + v_l \tag{35}$$

where

$$H_l = H_2 + H_3 \tag{36a}$$

$$H_2 = \begin{bmatrix} d_{\beta_l}\beta_x & d_{\beta_l}\beta_y & 0 \\ d_{\alpha_2}\alpha_x & d_{\alpha_2}\alpha_y & d_{\alpha_2}\alpha_z \end{bmatrix} \tag{36b}$$

$$H_3 = \begin{bmatrix} \dfrac{d_{12}}{R_N+H} - \dfrac{1}{R_E+H}(d_{11} + d_{13}\cdot\tan\lambda) & 0 \\ \dfrac{d_{22}}{R_N+H} - \dfrac{1}{R_E+H} d_{21} & 0 \end{bmatrix} \tag{36c}$$

$$H_4 = \begin{bmatrix} d_{11} & d_{12} & d_{13} \\ d_{21} & d_{22} & 0 \end{bmatrix} \tag{36d}$$

It is assumed that v_l is a zero mean white noise.

Another alternative is to express w and h as angular errors. To meet this end, Eq. (36) is divided by $r = |\bar{r}|$ which yields

$$\begin{bmatrix} \gamma_w \\ \gamma_h \end{bmatrix} = \frac{1}{r} \left[\begin{array}{c|c} H_l & H_4 \end{array}\right] \begin{bmatrix} \Delta r \\ \psi \end{bmatrix} + n \tag{37}$$

where

$$\gamma_w = w/r \qquad \gamma_h = h/r \tag{38}$$

γ_w and γ_h are the angular errors which correspond to w and h, respectively. Note that due to the smallness of w and h with respect to r, γ_w and γ_h are considered to be angles in radians rather than tangents of these angles. The observation error

vector n is now a vector of angular measurement errors. Another variant of this observation method is to lock the LOS on the landmark and measure the angles $-\gamma_w$ and $-\gamma_h$, at which the LOS has to be rotated about the z_{sc} and the y_{sc} axes, respectively, in order to shift the LOS to point L (see Fig. 2). Once the LOS is locked on the landmark another observation option exists as follows.

Mode II: Angular Tracking-Rate Error

Another way of using a landmark to update the INS is to lock the LOS on it, measure the yaw and pitch rates of the SD and subtract them from the corresponding INS-computed angular rates. The difference is a function of the INS errors. Linearizing this function and adding the observation noise yield the linear observation equation. This equation is derived next.

Note that Eq. (37) expresses the angular displacement error in the s_0 coordinate system of the SD; hence differentiation of Eq. (37), less the noise vector n, with respect to time yields the desired linear relation between the INS errors and the angular tracking-rate error in the SD coordinate system as follows

$$\Delta\omega=\begin{bmatrix}\dot\gamma_z\\ \dot\gamma_y\end{bmatrix}=\left[\frac{1}{r}H_1-\frac{V_r}{r}H_1\;\middle|\;H_1\;\middle|\;\dot H_4-\frac{V_r}{r}H_4\;\middle|\;H_4\right]\begin{bmatrix}x_1\\ \dot\psi\end{bmatrix} \tag{39a}$$

where $r=|r|$,

$$x_1^t=[\Delta r^t,\quad \Delta\dot r^t,\quad \psi^t] \tag{39b}$$

and

$$V_r=\mathrm{d}r/\mathrm{d}t \tag{39c}$$

The matrices $\dot H_1$ and $\dot H_2$ are derived from Eq. (36). Define H_{21}, H_{22}, H_{23}, and H_{24} as follows:

$$H_{21}=\begin{bmatrix}\dot d_{\beta_1}\beta_x & \dot d_{\beta_1}\beta_y & 0\\ \dot d_{\alpha_2}\alpha_x & \dot d_{\alpha_2}\alpha_y & d_{\alpha_2}\alpha_z\end{bmatrix} \tag{40}$$

$$H_{22}=\begin{bmatrix}d_{\beta_1}\dot\beta_x & d_{\beta_1}\dot\beta_y & 0\\ d_{\alpha_2}\dot\alpha_x & d_{\alpha_2}\dot\alpha_y & d_{\alpha_2}\dot\alpha_z\end{bmatrix} \tag{41}$$

$$H_{31}=\begin{bmatrix}\dfrac{\dot d_{11}}{R_N+H} & -\dfrac{1}{R_E+H}\left(\dot d_{11}+\dot d_{13}\tan\lambda+d_{13}\dfrac{\dot\lambda}{\cos^2\lambda}\right) & 0\\ \dfrac{\dot d_{22}}{R_N+H} & -\dfrac{1}{R_E+H}\dot d_{21} & 0\end{bmatrix} \tag{42}$$

$$H_{32}=\begin{bmatrix}d_{12}b_1 & -(d_{11}+d_{13}\tan\lambda)\,b_2 & 0\\ d_{22}b_1 & -d_{21}b_2 & 0\end{bmatrix} \tag{43}$$

where

$$b_1=-(\dot R_N+V_z)/(R_N+H)^2 \tag{44a}$$

$$b_2=-(\dot R_E+V_z)/(R_E+H)^2 \tag{44b}$$

$$\dot R_E=R_o e\sin(2\lambda)\dot\lambda \tag{45a}$$

$$\dot R_N=3\dot R_E \tag{45b}$$

$$\dot\lambda=V_x/(R_N+H) \tag{45c}$$

and where R_o is the radius of the Earth at the Equator and e is its ellipticity.

The time derivatives introduced in Eqs. (40-42) are evaluated in Appendix A. Now, from Eq. (36) it is realized that

$$H_1=H_{21}+H_{22}+H_{31}+H_{32} \tag{46}$$

and from Eq. (36d),

$$H_4=\begin{bmatrix}\dot d_{11} & \dot d_{12} & \dot d_{13}\\ \dot d_{21} & \dot d_{22} & 0\end{bmatrix} \tag{47}$$

The time derivatives in Eq. (47) are evaluated in Appendix A. Adding the observation noise vector v_2, the observation equation for this mode is obtained as follows

$$\Delta\omega=\frac{1}{r}\left[\dot H_1-\frac{V_r}{r}H_1\;\middle|\;H_1\;\middle|\;\dot H_4-\frac{V_r}{r}H_4\;\middle|\;H_4\right]\begin{bmatrix}x_1\\ \dot\psi\end{bmatrix}+v_2 \tag{48}$$

It is well known[5,6] that

$$\overline{\Delta\dot r}=\overline{\Delta V}-\bar\rho\times\overline{\Delta r} \tag{49}$$

where $\bar\rho$ is the vector of angular velocity at which the local-level local-north coordinate system rotates with respect to a Cartesian coordinate system fixed to the Earth. Using the following notation

$$[\rho]=\begin{bmatrix}0 & -\rho_z & \rho_y\\ \rho_z & 0 & -\rho_x\\ -\rho_y & \rho_x & 0\end{bmatrix} \tag{50}$$

Eq. (49) can be written as

$$\Delta\dot r=\Delta V-[\rho]\Delta r \tag{51}$$

and then Eq. (48) can be written as

$$\Delta\omega=\frac{1}{r}\left[\dot H_1-\frac{V_r}{r}H_1-H_1[\rho]\;\middle|\;H_1\;\middle|\;\dot H_4-\frac{V_r}{r}H_4\;\middle|\;H_4\right]\cdot\begin{bmatrix}x_2\\ \dot\psi\end{bmatrix}+v_2 \tag{52a}$$

where

$$x_2^t=[\Delta r^t,\quad \Delta V^t,\quad \psi^t] \tag{52b}$$

Finally, if the measured angular velocities are those of the SD gimbals (viz., $\dot\beta$ and $\dot\alpha$) then Eq. (52a) can be adjusted accordingly using the relations

$$\dot\gamma_z=\cos\alpha\cdot\Delta\dot\beta \tag{53a}$$

$$\dot\gamma_y=\Delta\dot\alpha \tag{53b}$$

III. INS Linear Error Propagation Model

The INS linearized differential equations, which describe the propagation of the system error, are well documented.[5,7] In this work the following version is used:

$$\overline{\Delta\dot r}=\overline{\Delta V}-\bar\rho\times\overline{\Delta r} \tag{54a}$$

$$\overline{\Delta \dot{V}} = -(2\bar{\Omega}+\bar{\rho}) \times \overline{\Delta V} + \overline{\Delta g} - \bar{\psi} \times \bar{a} + \overline{\nabla} \tag{54b}$$

$$\overline{\dot{\psi}} = -(\bar{\Omega}+\bar{\rho}) \times \bar{\psi} + \bar{\epsilon} \tag{54c}$$

where $\bar{\Omega}$ is the Earth rate vector, $\overline{\Delta g}$ is the gravity error vector, $\bar{a}$ is the sensed specific force vector, ∇ is a vector of accelerometer errors, and $\bar{\epsilon}$ is a vector of gyro drift rates. Using the matrix notation for a vector cross product [see Eq. (50)], Eq. (54) can be written as

$$\dot{x}_2 = Bx_2 + w \tag{55}$$

where

$$B = \begin{bmatrix} -[\rho] & I & 0 \\ G & -[2\Omega+\rho] & -[a] \\ 0 & 0 & -[\Omega+\rho] \end{bmatrix} \tag{56}$$

$$G = \frac{g_e R_e^2}{(R_e+H)^3} \begin{bmatrix} -1 & 0 & 0 \\ 0 & -1 & 0 \\ 0 & 0 & +2 \end{bmatrix} \tag{57}$$

and

$$w^t = [0,0,0,\nabla_x,\nabla_y\nabla_z,\epsilon_x,\epsilon_y,\epsilon_z] \tag{58}$$

The subscript e in Eq. (57) denotes the fact that g and R are, respectively, the gravity and the radius of the Earth computed on an elliptical Earth model and correspond to the geographic location of the vehicle.

For the accuracy required in this work it is sufficient to model the accelerometer error vector as a sum of a vector of random constants and a vector of random zero mean white noise signals. The same model is assumed also for the gyro drifts, hence

$$\nabla = \nabla_0 + w_\nabla \tag{59a}$$

$$\epsilon = \epsilon_0 + w_\epsilon \tag{59b}$$

$$\dot{\nabla}_0 = 0 \tag{60a}$$

$$\dot{\epsilon}_0 = 0 \tag{60b}$$

where ∇_0 and ϵ_0 are, obviously, the constant vectors and w_∇ and w_ϵ are the zero mean white noise vectors.

Augmentation of Eqs. (55, 59, and 60) yields the INS error propagation model

$$\dot{x} = Ax + w \tag{61}$$

where

$$x^t = [\Delta x,\Delta y,\Delta z,\Delta V_x,\Delta V_y,\Delta V_z,\psi_x\psi_y,\psi_z,$$
$$\nabla_{x0},\nabla_{y0},\nabla_{z0},\epsilon_{x0},\epsilon_{y0},\epsilon_{z0} \tag{62}$$

$$A = \left[\begin{array}{ccc:c:cc} & & & 0 & 0 \\ & B & & I & 0 \\ & & & 0 & I \\ \hline 0 & 0 & 0 & 0 & 0 \\ \hline 0 & 0 & 0 & 0 & 0 \end{array}\right] \tag{63}$$

and

$$w^t = [0,0,0,w_{\nabla x},w_{\nabla y},w_{\nabla z},w_{\epsilon x},w_{\epsilon y},w_{\epsilon z},0,0,0,0,0,0] \tag{64}$$

The vector w contains only zero mean white noise processes uncorrelated with one another.

IV. Filter Formulation

The preceeding developments indicate that the basic INS error propagation model as well as the observation model are nonlinear. However, the linearized models lend themselves to the application of the extended Kalman filter algorithm for estimating the INS errors and error sources, based on the observation modes discussed heretofore. The extended Kalman filter has been well documented[8,9] and will not be outlined here, only the most relevant equations will be listed. It should be noted that on board the vehicle the linearization is performed about the best available estimate of the trajectory.[3,10] In this study, however, the analysis is based on covariance matrix propagation and update. Therefore the state itself is not estimated and, hence, the nominal trajectory rather than the best estimate of the actual trajectory is used in the linearization.[3]

For the first observation mode the covariance analysis is based on the following algorithm[8]:

Between Observations:

$$P_{k+1}(-) = \Phi_k P_k(+)\Phi_k^t + Q_k \tag{65a}$$

$$P_{k+1}(+) = P_{k+1}(-) \tag{65b}$$

where Φ_k is the transition matrix from the time point t_k to t_{k+1} based on A of Eq. (63) and Q_k is the discrete-time value of the covariance matrix of the white noise vector w given in Eq. (64). To find Q_k, define the diagonal matrix Q as

$$Q = \text{diag}[0,0,0,\sigma^2_{w_{\nabla x}},\sigma^2_{w_{\nabla y}},\sigma^2_{w_{\nabla z}},\sigma^2_{w_{\epsilon x}},\sigma^2_{w_{\epsilon y}},\sigma^2_{w_{\epsilon z}},0,0,0,0,0,0] \tag{65c}$$

Now divide the interval (t_k,t_{k+1}) into N equal steps of length Δt and let $A_i = A(t_k+i\Delta t)$. Then following equations (8.3-24) in Ref. 9, the value for Q_k is given by

$$Q_k = NQ\Delta t + \left(\sum_{i=1}^{N-1} iF_i\right)Q\Delta t^2 + Q\Delta t^2\left(\sum_{i=1}^{N-1} iF_i^t\right) \tag{65d}$$

Across an Observation:

Use Eq. (65a) to compute $P_{k+1}(-)$, and then compute

$$P_{k+1}(+) = [I-K_{k+1}H_{k+1}]P_{k+1}(-)[I-K_{k+1}H_{k+1}]^t + K_{k+1}R_{k+1}K_{k+1}^t \tag{66}$$

where

$$K_{k+1} = P_{k+1}(-)H_{k+1}^t \cdot [H_{k+1}P_{k+1}(-)H_{k+1}^t + R_{k+1}]^{-1} \tag{67}$$

H_{k+1} is the 2×15 matrix

$$H_{k+1} = [H_1\,|0|\,H_4\,|0]\text{---}|0]_{k+1} \tag{68}$$

in which H_1 and H_4, which are given in Eq. (36), are evaluated, for the nominal trajectory, at t_{k+1}, and the 0 matrix is a 2×3 matrix of zeros. R_{k+1} is the covariance matrix of the observation error vector v_1 of Eq. (35).

The observation equation of the second mode, i.e., for Eq. (52), introduces some difficulty since $\dot{\psi}$ is not a part of the state vector. This difficulty can be overcome as follows.

Rewrite Eq. (52) as

$$\Delta\omega = \left[H_5 \left| \frac{1}{r} H_1 \right| H_6\right] x_2 + \frac{1}{r} H_4 \dot{\psi} + v_2 \tag{69a}$$

where

$$H_5 = \frac{1}{r}\left[\dot{H}_1 - \frac{V_r}{r} H_1 - H_1[\rho]\right] \tag{69b}$$

and

$$H_6 = \frac{1}{r}\left[\dot{H}_4 - \frac{V_r}{r} H_4\right] \tag{69c}$$

Now, using Eqs. (54c) and (59b) it is obvious that

$$\frac{1}{r} H_4 \dot{\psi} = -\frac{1}{r} H_4 [\Omega + \rho]\psi + \frac{1}{r} H_4 \epsilon_0 + \frac{1}{r} H_4 w_\epsilon \tag{70}$$

which, when substituted into Eq. (69a) yields

$$\Delta\omega = \left[H_5 \left| \frac{1}{r} H_1 \right| H_6 - \frac{1}{r} H_4 [\Omega + \rho] \,|0| \frac{1}{r} H_4\right] x + \left(v_2 + \frac{1}{r} H_4 w_\epsilon\right) \tag{71}$$

The last observation equation does not include a direct dependence on $\dot{\psi}$ anymore; however, the observation noise in this equation is now a linear combination of v_2 and w_ϵ, and thus it is correlated with w, the white noise of the INS error-propagation model. This case has been treated in the literature. For example, Ref. 8 treats the discrete and the continuous cases, Ref. 9 the continuous case, and Ref. 11 treats both cases. Define Q_{ϵ_k} as follows:

$$\text{cov}\{w_{\epsilon k},\ w^t_{\epsilon_j}\} = Q_{\epsilon_k} \delta_{k,j} \tag{72}$$

where $\delta_{k,j} = 1$ for $k = j$ and is zero otherwise. Then it can be shown that

$$\text{cov}\{w_k,\ (v_{2_j} + \frac{1}{r_j} H_{4_j} w_{\epsilon_j})^t\}^t = \left[0|0|0|\left(\frac{1}{r_j} Q_{\epsilon_k} H^t_{4_j}\right)^t |0\right]\delta_{k,j} \tag{73}$$

which is a 2×15 matrix.

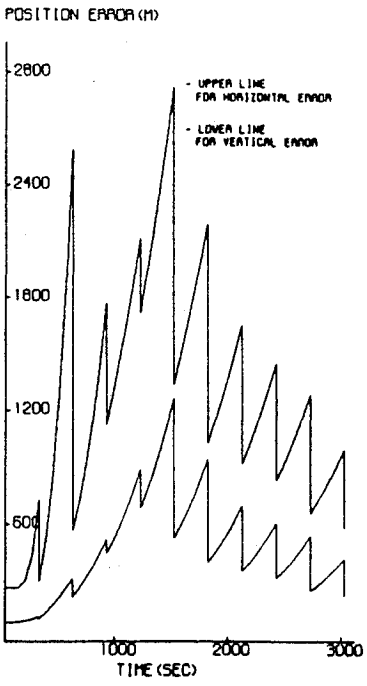

Fig. 3 Position error propagation for single-sided observations of the first mode (one update every 5 min).

Following Ref. 8 the algorithm for this case is as follows.

Between observations define a 2×15 matrix

$$\Sigma^t_k = \left[0|0|0|\left(\frac{1}{r_k} Q_{\epsilon_k} H^t_{4_k} R_k^{-t}\right)^t |0\right] \tag{74}$$

then, if there is an observation update at k, use

$$P_{k+1}(-) = [\phi_k - \Sigma_k H_k] P_k(+) [\phi_k - \Sigma_k H_k]^t + Q_k - \Sigma_k R_k \Sigma^t_k \tag{75}$$

$$P_{k+1}(+) = P_{k+1}(-) \tag{76}$$

where

$$H_k = \left[H_5 \left| \frac{1}{r} H_1 \right| H_6 - \frac{1}{r} H_4 [\Omega + \rho] \,|0| \frac{1}{r} H_4\right]_k \tag{77}$$

and if there is no observation update at k, use Eq. (65). Across an observation use Eqs. (74) and (75) [or Eq. (65a) if there was no observation update at k] to compute $P_{k+1}(-)$, and then use Eqs. (66) and (67) to compute $P_{k+1}(+)$ where H_{k+1} is, of course, Eq. (77) evaluated at t_{k+1}.

V. Results of Covariance Analysis

The covariance matrix of the estimation error was propagated, and updated at observations. The propagation was carried out along a trajectory characterized by a cruising speed of 300m/s and a cruising altitude of 3000 m. Observations were made, typically, at 5-min intervals. The following 1σ values of the initial errors were used:

$\Delta x = 200$ m	$\Delta y = 200$ m	$\Delta z = 100$ m
$\Delta V_x = 0.1$ m/s	$\Delta V_y = 0.1$ m/s	$\Delta V_z = 0.1$ m/s
$\psi_x = 1.0$ arc-min	$\psi_y = 1.0$ arc-min	$\psi_z = 3.0$ arc-min
$\nabla_{x_0} = 100\,\mu g$	$\nabla_{y_0} = 100\,\mu g$	$\nabla_{z_0} = 100\,\mu g$
$\epsilon_{x_0} = 2.04$ deg/h	$\epsilon_{y_0} = 2.04$ deg/h	$\epsilon_{z_0} = 2.04$ deg/h

The 1σ observation error was a 10-m horizontal and a 10-m vertical error in the observation of the landmark in the "image plane." Figure 3 displays the propagation of the vertical and the horizontal position errors. The mode of observation was the first one, namely, observation of errors in the image plane. One update was made at each updating point. At each such point the landmark was observed at an azimuth of 22 deg from the vehicle heading. Figure 4 displays the same, with the only difference that here the azimuth to the observed landmark was, alternately, ± 22 deg from the

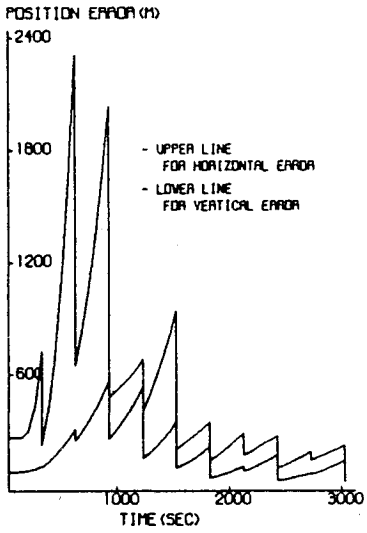

Fig. 4 Position error propagation for double-sided observations of the first mode (one update every 5 min).

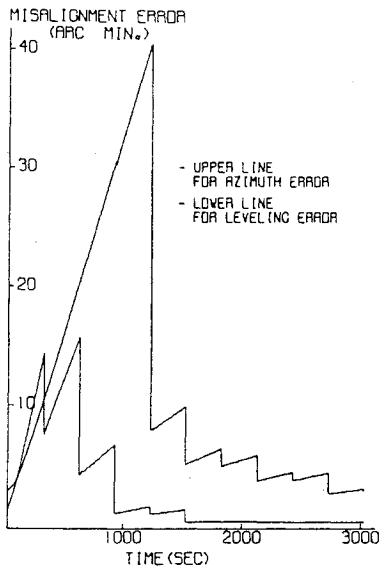

Fig. 5 Misalignment error propagation for double-sided observations of the first mode (one update every 5 min).

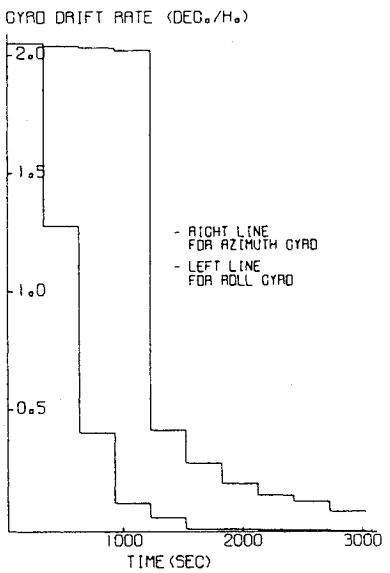

Fig. 6 Gyro drift rate propagation for double-sided observations of the first mode (one update every 5 min).

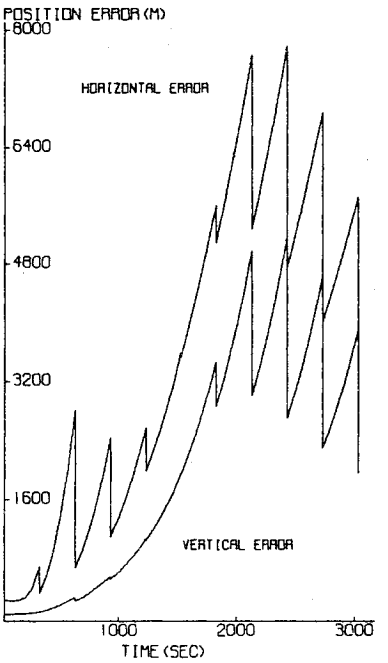

Fig. 7 Position error propagation for single-sided observations of the second mode (5 updates at the end of each 5-min interval).

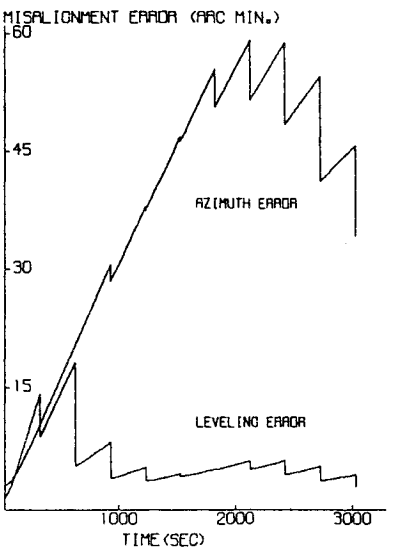

Fig. 8 Misalignment error propagation for single-sided observations of the second mode (5 updates at the end of each 5-min interval).

vehicle heading. Still, one observation and hence one update were made at each updating point. Figure 5 displays the behavior of the misalignment error (which corresponds to Fig. 4) whereas Fig. 6 displays the corresponding behavior of the gyro drift rates. The pitch gyro drift rate, not displayed in Fig. 6, behaves basically like the roll gyro drift rate. When two updates, each using a different landmark, were made at each updating point, that is, two updates at the end of each 5-min interval, the performance of the hybrid system was remarkably better, as expected.

Figure 7 displays the position error propagation when the observation is of the second mode. The SD tracks a target at 5-s periods which are spaced in time 5 min apart. During the 5-s periods, 5 observations and updates are made, one at the end of each second. The landmarks which are being tracked are all at the same azimuth from the vehicle heading. Figure 8 displays the corresponding misalignment error propagation and Fig. 9, the propagation of the corresponding gyro drift rates.

VI. Conclusion

Two updating modes of a low-accuracy INS, utilizing information obtained from a sighting device, were considered. The observation equations for the two modes were developed and linearized. An extended Kalman filter was designed for both modes. It turns out that when rate information is observed, that is, when the second updating mode is used, a part of the observation noise vector is correlated with a part of the state-equation noise vector. This fact adds some complexity to the filter algorithm.

A covariance analysis was carried out which verified the efficiency of the hybrid system. It was found, as expected, that the observability of the system was better, and hence the error check was superior, when the observed landmarks were on both sides of the trajectory and/or updates were performed more frequently. The combination of the first and second updating modes also reduced the INS errors. This fact, however, is not the main quality of the second updating mode. Its main advantage stems, rather, from the fact that when the second mode is used to update the INS it is not necessary to predetermine and later identify the landmarks observed by the SD. It is sufficient to lock the LOS on a well-distinguished landmark, and as long as the INS errors are not too large, the measured azimuth and depression angles to the landmark produce sufficient and accurate enough data for the Kalman filter algorithm of this mode.

Finally, it should be pointed out that, formally, a Kalman filter error analysis[9] should have been carried out to confirm

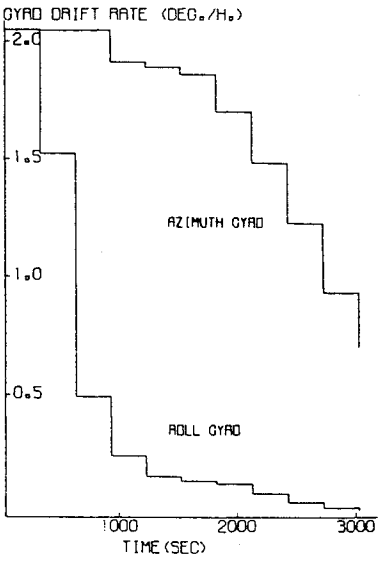

Fig. 9 Gyro drift rate propagation for single-sided observations of the second mode (5 updates at the end of each 5-min interval).

the results and to verify that the 15-state INS error model is an accurate enough representation of the "real world" INS error. However, it was indicated in the past (see, for example, Ref. 12) that for an aided INS, whose accuracy is similar to that achieved in this work, a 15-state model is sufficient.

Appendix

The purpose of this appendix is to develop the expressions for the time derivatives introduced in Eqs. (40-42) and in Eq. (47). Differentiation of Eq. (27) with respect to time yields

$$\dot{d}_{\beta 1} = S\beta_0 \cdot (x_L - x_0)\,\dot{\beta}_0 + C\beta_0 \cdot V_x - C\beta_0 \cdot (y_L - y_0)\,\dot{\beta}_0 + S\beta_0 \cdot V_y \tag{A1}$$

Similarly, from Eq. (29)

$$\begin{aligned}\dot{d}_{\alpha_2} = &-S\beta_0 \cdot C\alpha_0 \cdot (x_L - x_0) \cdot \dot{\beta}_0 \\ &- C\beta_0 \cdot S\alpha_0 \cdot (x_L - x_0) \cdot \dot{\alpha}_0 \\ &- C\beta_0 \cdot C\alpha_0 \cdot V_x + C\beta_0 \cdot C\alpha_0 \cdot (y_L - y_0) \cdot \dot{\beta}_0 \\ &- S\beta_0 \cdot S\alpha_0 \cdot (y_L - y_0) \cdot \dot{\alpha}_0 - S\beta_0 \cdot C\alpha_0 \cdot V_y \\ &- C\alpha_0 \cdot (z_L - z_0) \cdot \dot{\alpha}_0 + S\alpha_0 \cdot V_z\end{aligned} \tag{A2}$$

The expression for $\dot{\beta}_0$ is obtained from Eq. (22) as

$$\dot{\beta}_0 = \beta_x V_x + \beta_y V_y \tag{A3}$$

and that for $\dot{\alpha}_0$ is obtained from Eq. (24) as

$$\dot{\alpha}_0 = \alpha_x V_x + \alpha_y V_y + \alpha_z V_z$$

To obtain $\dot{\beta}_x$ differentiate Eq. (23a), thus,

$$\dot{\beta}_x = \frac{C(2\beta_0)}{(x_L - x_0)}\,\dot{\beta}_0 + \frac{S(2\beta_0)}{2(x_L - x_0)^2}\,V_x \tag{A4}$$

and similarly, from Eq. (23b)

$$\beta_y = \frac{S(2\beta_0)}{x_L - x_0}\,\dot{\beta}_0 - \frac{C^2\beta_0}{(x_L - x_0)^2}\,V_x \tag{A5}$$

Now, from Eq. (25a)

$$\dot{\alpha}_x = \frac{(x_L - x_0)C^2\alpha_0}{d_0^3}\,V_z - \frac{(z_0 - z_L)C^2\alpha_0}{d_0^3}\,V_x$$

$$- \frac{(z_0 - z_L)(x_L - x_0) \cdot S(2\alpha_0)}{d_0^3}\,\dot{\alpha}_0$$

$$+ 3\,\frac{(z_0 - z_L)(x_L - x_0)C^2\alpha_0[(x_L - x_0)V_x + (y_L - y_0)V_y]}{d_0^5} \tag{A6}$$

from Eq. (25b)

$$\dot{\alpha}_y = \frac{(y_L - y_0)C^2\alpha_0}{d_0^3}\,V_z - \frac{(z_0 - z_L)C^2\alpha_0}{d_0^3}\,V_y$$

$$- \frac{(z_0 - z_L)(y_L - y_0) \cdot S(2\alpha_0)}{d_0^3}\,\dot{\alpha}_0$$

$$+ 3\,\frac{(z_0 - z_L)(y_L - y_0)C^2\alpha_0[(x_L - x_0)V_x + (y_L - y_0)V_y]}{d_0^5} \tag{A7}$$

and from Eq. (25c)

$$\dot{\alpha}_z = -\frac{S(2\alpha_0)}{d_0}\,\dot{\alpha}_0 + \frac{C^2\alpha_0[(x_L - x_0)V_x + (y_L - y_0)V_y]}{d_0^3} \tag{A8}$$

Finally, from Eq. (31)

$$\dot{d}_{11} = -S\beta_0 \cdot (z_L - z_0) \cdot \dot{\beta}_0 - C\beta_0 \cdot V_z \tag{A9}$$

$$\dot{d}_{12} = C\beta_0 \cdot (z_L - z_0) \cdot \dot{\beta}_0 - S\beta_0 \cdot V_z \tag{A10}$$

$$\dot{d}_{13} = \dot{d}_{\beta 1} \tag{A11}$$

$$\begin{aligned}d_{21} = &\,C\beta_0 \cdot S\alpha_0 \cdot (z_L - z_0) \cdot \dot{\beta}_0 + S\beta_0 \cdot C\alpha_0 \cdot (z_L - z_0) \cdot \dot{\alpha}_0 \\ &- S\beta_0 \cdot S\alpha_0 \cdot V_z + S\alpha_0 \cdot (y_L - y_0) \cdot \dot{\alpha}_0 + C\alpha_0 \cdot V_y\end{aligned} \tag{A12}$$

$$\begin{aligned}\dot{d}_{22} = &-S\alpha_0 \cdot (x_L - x_0) \cdot \dot{\alpha}_0 - C\alpha_0 \cdot V_x + S\beta_0 \cdot S\alpha_0 \cdot (z_L - z_0) \\ &\cdot \dot{\beta}_0 - C\beta_0 \cdot C\alpha_0 \cdot (z_L - z_0) \cdot \dot{\alpha}_0 + C\beta_0 \cdot S\alpha_0 \cdot V_z\end{aligned} \tag{A13}$$

This completes the development of the expressions for the time derivatives introduced in Eqs. (40-42) and in Eq. (47).

Acknowledgment

The author wishes to express his gratitude to A. Yavnai and particularly to A. Weinreb for their inspiring discussions and for their help in reviewing this work.

References

[1] Bryson, A.E. Jr. and Ho, Y.C., *Applied Optimal Control,* Blaisdell Publishing Co., Waltham, Mass., 1969, Chap. 12.

[2] Mackison, D.L. and Gutshall, R.L., "Star-Scanner Attitude Determination for the OSO-F Spacecraft," *Journal of Spacecraft and Rockets,* Vol. 10, April 1973, pp. 262-267.

[3] White, R.L., Adams, M.B., Geisler, E.G., and Grant, F.D., "Attitude Estimation Using Stars and Landmarks," *IEEE Transactions on Aerospace and Electronic Systems,* Vol. AES-11, March 1975, pp. 195-203.

[4] Farrell, J.L., *Integrated Aircraft Navigation,* Academic Press, New York, 1976, Chap. 7,8.

[5] Pitman, G.R. (ed.), *Inertial Guidance,* Wiley, New York, 1962.

[6] Leondes, C.T. (ed.), *Guidance and Control of Aerospace Vehicles,* McGraw-Hill, New York, 1963.

[7] Broxmeyer, C., *Inertial Navigation Systems,* McGraw-Hill, New York, 1964.

[8] Sage, A.P. and Melsa, J.L., *Estimation Theory with Applications to Communications and Control,* McGraw-Hill, New York, 1971.

[9] Gelb, A. (ed.), *Applied Optimal Estimation,* M.I.T. Press, Cambridge, Mass., 1974.

[10] Bennett, J.E. and Hung, J.C., "Application of Statistical Techniques to Landmark Navigation," *Navigation, Journal of the Institute of Navigation,* Vol. 17, Winter 1970-71, pp. 349-357.

[11] Kwakernaak, H. and Sivan, R., *Linear Optimal Control Systems,* Wiley-Interscience, New York, 1972.

[12] Wauer, J.C., "Practical Considerations in Implementing Kalman Filters," in "Practical Aspects of Kalman Filtering Implementation," NATO AGARD-LS-82, AD-A024, 377, March 1976, Chap. 2.